

Force and conductance during contact formation to a C₆₀ molecule

This article has been downloaded from IOPscience. Please scroll down to see the full text article.

2012 New J. Phys. 14 073032

(<http://iopscience.iop.org/1367-2630/14/7/073032>)

View [the table of contents for this issue](#), or go to the [journal homepage](#) for more

Download details:

IP Address: 158.227.172.11

The article was downloaded on 18/07/2012 at 17:07

Please note that [terms and conditions apply](#).

Force and conductance during contact formation to a C₆₀ molecule

Nadine Hauptmann^{1,4}, Fabian Mohn², Leo Gross²,
Gerhard Meyer², Thomas Frederiksen³ and Richard Berndt¹

¹ Institut für Experimentelle und Angewandte Physik,
Christian-Albrechts-Universität zu Kiel, D-24098 Kiel, Germany

² IBM Research—Zurich, CH-8803 Rüschlikon, Switzerland

³ Donostia International Physics Center (DIPC)-UPV/EHU, E-20018
Donostia-San Sebastián, Spain

E-mail: hauptmann@physik.uni-kiel.de

New Journal of Physics **14** (2012) 073032 (14pp)


Received 15 February 2012

Published 13 July 2012

Online at <http://www.njp.org/>

doi:10.1088/1367-2630/14/7/073032

Abstract. Force and conductance were simultaneously measured during the formation of Cu–C₆₀ and C₆₀–C₆₀ contacts using a combined cryogenic scanning tunneling and atomic force microscope. The contact geometry was controlled with submolecular resolution. The maximal attractive forces measured for the two types of junctions were found to differ significantly. We show that the previously reported values of the contact conductance correspond to the junction being under maximal tensile stress.

 Online supplementary data available from stacks.iop.org/NJP/14/073032/mmedia

⁴ Author to whom any correspondence should be addressed.

Contents

1. Introduction	2
2. Experiment	3
3. Cu–C₆₀ contacts	3
4. C₆₀–C₆₀ contacts	5
5. Comparison of elasticities of Cu–C₆₀ and C₆₀–C₆₀ contacts	7
6. Conclusions	8
Acknowledgments	8
Appendix A. Density functional theory calculations	9
Appendix B. Elasticity model	12
References	13

1. Introduction

When a molecule is contacted by electrodes to measure the conductance of the molecular junction, new bonds are formed and significant forces may arise. These forces affect the atomic-scale junction geometry, which is crucial for its transport properties [1–5]. The current and force can be measured simultaneously using a combination of scanning tunneling microscopy (STM) and atomic force microscopy (AFM). Such measurements were carried out for metallic contacts [2, 6–9]. Related data were reported for contacts to single molecules in a liquid environment [10, 11] and for molecules on a metal surface [12]. However, the exact contact geometry was not accessible. 3,4,9,10-Perylene-tetracarboxylicacid-dianhydride was probed in ultrahigh vacuum using AFM to controllably lift the molecule [13]. A bimodal distribution of conductances was observed and suggested to reflect two distinct bonding geometries. As to controlled molecule–molecule contacts, experimental results are few. The conductance of C₆₀–C₆₀ contacts was measured by attaching a C₆₀ molecule to an STM tip and approaching a second molecule in a monolayer on Cu(111) [14]. The force between a metal tip and C₆₀ molecules in double layers on Cu(111) was addressed with AFM [16, 17]. While close distances well into the repulsive range were explored, the corresponding conductances⁵ were significantly lower than in the STM work of [14]. A possible origin of this difference may be the different geometries of the contact between the tip and the molecule in these experiments. Atomically sharp electrodes were shown to act as bottlenecks for charge injection into C₆₀ [15, 18]. While tips had been intentionally flattened to firmly attach a molecule in [14], the tip used in [16] presumably was atomically sharp. Another possible reason for reduced conductance is foreign material at the tip apex. Here, we present low-temperature force and conductance data for the controlled formation of Cu–C₆₀ and C₆₀–C₆₀ contacts. The orientations of the molecules at the tip and the surface were determined from STM imaging. The elasticity of both the contacts is analyzed and compared using density functional theory (DFT) calculations.

⁵ The current shown in [16] appears to represent the average over an oscillation cycle of the vibrating AFM tip. From these data the instantaneous current at the point of closest approach of the tip to the sample, which may be compared with the current in an STM, can be estimated using the method of Sader and Sugimoto [25].

2. Experiment

Our experiments were performed with a homebuilt STM/AFM in ultrahigh vacuum at a temperature of 5 K. Clean Cu(111) surfaces were prepared by repeated sputtering and annealing cycles. Submonolayer amounts of C_{60} were then deposited onto the sample by sublimation at room temperature. Subsequent annealing to ≈ 500 K led to a well-ordered 4×4 structure of C_{60} [19–22]. After additional sublimation of small amounts of C_{60} onto the cooled sample, isolated C_{60} molecules were found on both the C_{60} islands and the bare Cu substrate [23]. A PtIr tip was attached to the free prong of a quartz tuning fork oscillating with an amplitude of (3 ± 0.2) Å at its resonance frequency of ~ 28 kHz. The tip was covered with Cu by repeated indenting into the substrate until submolecular resolution was achieved. The vertical force F acting on the tip at the point of closest tip approach was calculated from the measured frequency shift $\Delta f(\Delta z)$ (shown in S1) as a function of the vertical piezo displacement Δz using the formalism of Sader and Jarvis [24]. Due to the limited bandwidth of the transimpedance amplifier, the current recorded with the oscillating tip is averaged over the entire range of oscillations. The non-averaged conductance $G(\Delta z)$ was calculated by the method of Sader and Sugimoto [25], which recovers the instantaneous current at the point of the closest tip approach. The bias voltage V was applied to the sample. Further experimental details can be found in the supplementary data (available from stacks.iop.org/NJP/14/073032/mmedia).

We note that the intrinsic energy dissipation of the tuning fork did not change significantly during the contact formation. In addition, STM images taken before and after the contact measurement showed no changes. These facts suggest that no inelastic deformations of the tip or the molecule occurred.

3. Cu– C_{60} contacts

Figure 1(a) displays a typical constant-current STM image of a C_{60} island used for contact measurements with Cu-covered tips. The island comprises two domains that differ by an azimuthal rotation of the h- C_{60} molecules by 60° (h0 and h60). C_{60} molecules adsorbed on Cu(111) with either a hexagon (h- C_{60}) or a pentagon (p- C_{60}) facing up give rise to distinctly different patterns in the STM image [26]. Figure 1(b) shows the different orientations of the molecules as viewed from the tip position. Double bonds separating two hexagons (6 : 6 bonds) are marked by red bars. Contact data recorded with a Cu tip above the center of a h- C_{60} molecule are shown in figure 1(c). Both the total interaction force F (solid line) evaluated at the point of closest approach to the sample and the instantaneous conductance G (dots) are displayed versus the piezo displacement Δz . We first focus on the force, which is shown over a wider range of displacements in figure 1(d). To minimize the electrostatic force, which results from the contact potential difference, a bias voltage of $V = 0.1$ V was applied during the contact measurement [27–29]. At large tip–sample distances, F reflects the long-range van der Waals force between the tip and the sample. It can be approximated by a power law $F_1(\Delta z) = a(\Delta z_0 - \Delta z)^b$ [30] with typical fit parameters $a = -5.5$ nN/Å^b, $b = -2.3$ and $\Delta z_0 = 7.5$ Å (fit range: $\Delta z \leq 0$ Å). The fit is shown in figure 1(d) as a dashed line. The exponent close to 2 indicates an effective sphere–plane geometry of the junction.

The short-range force $F_s(\Delta z)$ (dashed-dotted line in figure 1(d)), which only acts on the atoms in the immediate vicinity of the molecular junction, is estimated as $F_s = F - F_1$. It is attractive for large tip heights, reaches a minimum at $\Delta z \approx 4.8$ Å and finally becomes

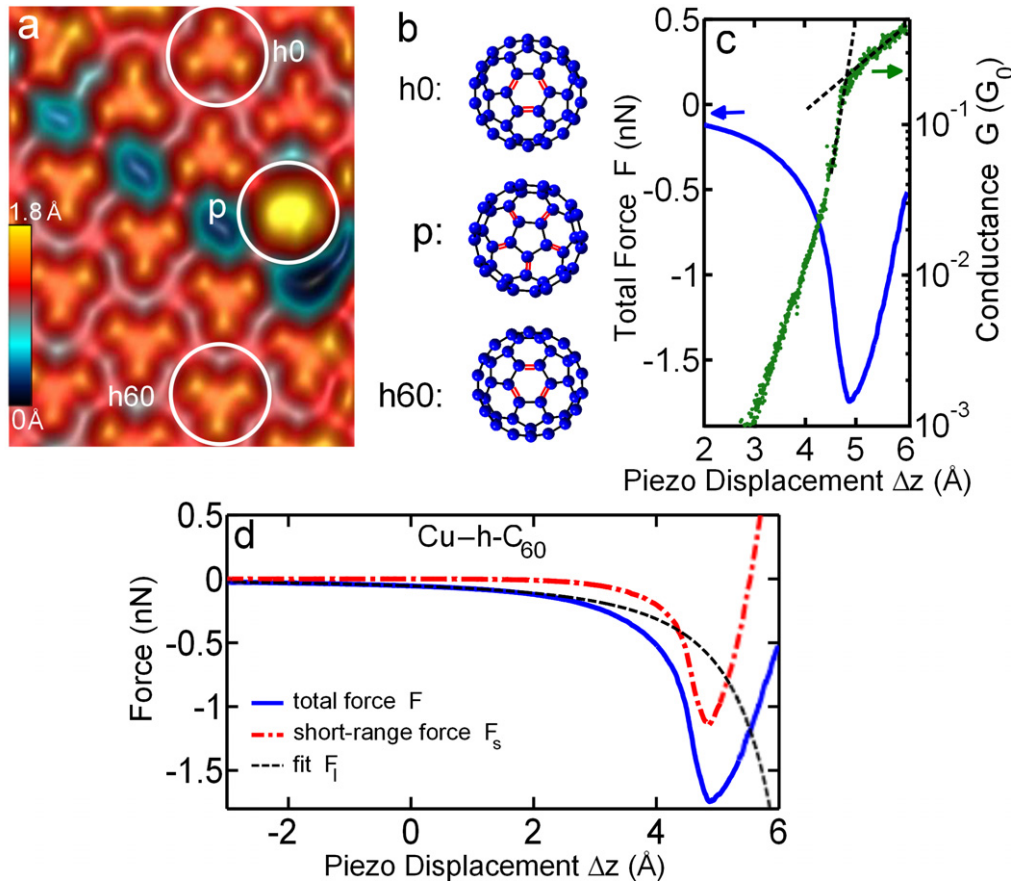


Figure 1. (a) Pseudo-three-dimensional (pseudo-3D) illuminated constant-current STM image (1.7 V, 0.55 nA, $3.8 \times 5 \text{ nm}^2$) of a C_{60} island showing three different molecule orientations (h0, p and h60). (b) Sketches of three orientations of C_{60} on Cu(111) as viewed from the tip. Red double bars indicate the bonds separating two hexagons (6 : 6 bonds). (c) Total force F (solid line) and instantaneous conductance G (dots) calculated from the simultaneously measured frequency shift and averaged conductance (figure S1, available from stacks.iop.org/NJP/14/073032/mmedia) using [24, 25]. A voltage of $V = 0.1 \text{ V}$ was applied to the sample. The oscillation amplitude of the tuning fork was $A = (3 \pm 0.2) \text{ \AA}$. Dashed lines define the point of contact. (d) Total force F (solid line) over a wider range of piezo displacements than in panel (c), fitted long-range force F_1 (dashed line, fit range: $\Delta z \leq 0 \text{ \AA}$, see text for details) and short-range force $F_s = F - F_1$ (dashed-dotted line). $\Delta z = 0 \text{ \AA}$ corresponds to the position defined by the STM set-point $I = 0.55 \text{ nA}$ at $V = 1.5 \text{ V}$.

repulsive for $\Delta z > 5.5 \text{ \AA}$. The fitted van der Waals force at contact ($\approx 0.5 \text{ nN}$) is consistent with estimates for a sharp tip [31]. We note that the total force F and the short-range force F_s exhibit maximal attraction at nearly the same position Δz . In other words, long-range forces do not significantly affect the point of maximal attraction. However, they do affect the value of the maximal attraction. Using different tips we found it to scatter between 1.5 and 2.2 nN. We ascribe the origin of these significant short-range forces to the chemical bond formation

between the tip and the molecule. Interestingly, calculated interaction forces for a Si tip and C_{60} on Si(100) are in a very similar range (1.4–2.0 nN) [31]. The $F(\Delta z)$ data of h- C_{60} and p- C_{60} were very similar except for a shift of $\approx 0.4 \text{ \AA}$ along the abscissa due to the different apparent heights of the molecules. This apparent insensitivity to the detailed bonding geometry may be attributed to the high reactivity of 6 : 6 bonds. It causes the Cu atom at the tip apex to laterally relax [18]. As a result, a 6 : 6 bond is most likely contacted independent of the orientation of the molecule. The conductance $G(\Delta z)$ in figure 1(c) shows a typical transition from tunneling at small Δz to electrical contact. To define the point of contact, the intersection of linear fits in the transition and contact regimes is used (figure 1(c), dashed lines) [5]. The resulting contact conductance $G_c \approx 0.2G_0$ ($G_0 = 2e^2/h$ is the conductance quantum) is in agreement with previous experimental results [5, 14, 15]. Comparing the conductance data with the simultaneously measured force (figure 1(c), solid line), we find that the point of contact corresponds to the maximal attractive force. The same observation is made for C_{60} – C_{60} contacts (see below). A similar result has been reported from metal–metal point contacts, where a maximal attractive force was measured at $G \sim G_0$ [9]. Modeling of metallic contacts also suggests that the deformation of the junction is maximal at the point of contact formation [32, 33]. Recently, two-level fluctuations of the conductance on a μs time scale were reported from C_{60} on Cu(100) at the transition from tunneling to contact for a metal– C_{60} contact [34]. In the present case of a 4×4 structure of C_{60} on Cu(111), and at the rather low bias voltages used (0.1–0.3 V), such fluctuations were not observed [35].

4. C_{60} – C_{60} contacts

By approaching the tip sufficiently close, a single C_{60} molecule was attached to the tip apex. The orientation of such C_{60} tips was determined by ‘reverse imaging’ on small Cu clusters which had been deposited before from the tip onto the bare Cu(111) surface [14, 15]. Constant-current images of such a Cu cluster recorded at $V = -2 \text{ V}$ reveal the second lowest unoccupied orbital (LUMO + 1) of the molecule [14]. Compared to normal STM images of the LUMO + 1 (figure 1(a)), they show a mirror image of the molecule (for details see supplementary data, available from stacks.iop.org/NJP/14/073032/mmedia).

The relative orientations of the tip and sample C_{60} molecules strongly affect the conductance of the junction in the tunneling range. Figure 2(a) shows a C_{60} island imaged using a C_{60} -functionalized tip with a hexagon facing towards the surface (h- C_{60} tip). Similar to figure 1(a), the island comprises two rotational domains of h- C_{60} (h0 and h60), as well as a few p- C_{60} molecules. Owing to the different orientations, distinctly different patterns are observed with the h- C_{60} tip for h0, p and h60 molecules (figures 2(b)–(d)). For example, the center of h- C_{60} appears either as a maximum (h0) or as a minimum (h60) in the STM image. On p- C_{60} a threefold symmetry of the h- C_{60} tip is clearly discernible, which reflects the 5 : 6 bonds of the molecule at the tip. The symmetries of these patterns can be understood from a convolution of the local densities of electronic states (LDOS) of the tip and the sample. At $V = 1.6 \text{ V}$, electrons essentially tunnel from the highest occupied molecular orbital (HOMO) of the h- C_{60} tip to the lowest unoccupied molecular orbital (LUMO) of the molecule at the surface. A 2D convolution of these orbitals according to the orientations given in figure S2 is shown in figures 2(e)–(g) (for details see supplementary data). It reproduces the experimental data, with the best agreement obtained for the h0 pattern.

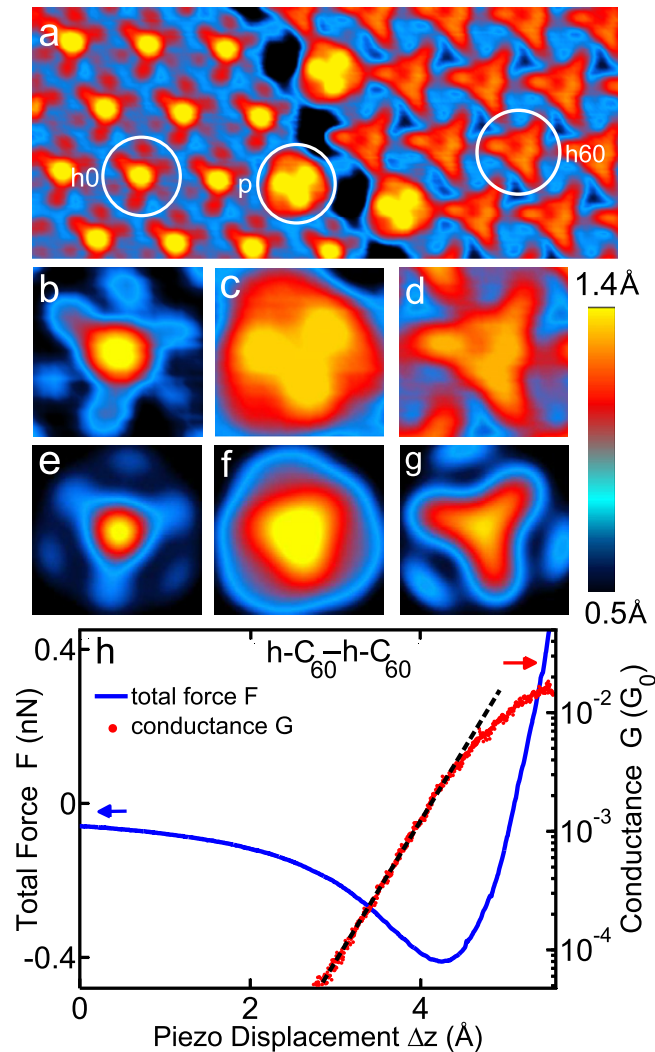


Figure 2. (a) Constant-current STM image (1.6 V, 0.55 nA $8 \times 4 \text{ nm}^2$) of a C_{60} island measured with a h-C_{60} tip. (b–d) Constant-current closeup images of molecules with orientations h0, p and h60, respectively. (e–g) Simulated images showing the convolution of the modeled local density of states (LDOS) of the HOMO of C_{60} at the tip and the LUMO of C_{60} at the surface for h0, p and h60 orientations, respectively (for details, see supplementary data, available from stacks.iop.org/NJP/14/073032/mmedia). (h) Instantaneous conductance G (dots) and the total force F (solid line) for the h-C_{60} – h-C_{60} contact calculated from the simultaneously measured frequency shift and averaged conductance (figure S1) using [24, 25]. An oscillation amplitude $A = (2.5 \pm 0.2) \text{ \AA}$ was used. A voltage $V = 0.3 \text{ V}$ was applied to the sample. The dashed line indicates an exponential fit to the conductance for small Δz .

Figure 2(h) displays the force (solid line) and the conductance (dots) measured on a h-C_{60} molecule with a h-C_{60} tip at an applied voltage of $V = 0.3 \text{ V}$. Compared to the data from a Cu tip (figure 1(c)), the maximal attractive force is smaller by a factor of 4. In experiments with

different C_{60} tips, this maximal attractive force varied from 0.3 to 0.4 nN. In part, this scatter may be attributed to the uncertainty of the lateral tip position, which we estimate to be $\approx 10\%$ of a C_{60} diameter. The conductance measured for a C_{60} – C_{60} contact (figure 2(h), dots) starts to deviate from purely exponential behavior (dashed line) at a piezo displacement close to the position of the maximum of the attractive force. The conductance at this point ($\approx 3 \times 10^{-3} G_0$) is approximately two orders of magnitude smaller than with a Cu tip [14]. When we approached the tip further towards the surface until the total force exceeded 0.5 nN, a rotation of the C_{60} molecule at the tip occurred.

5. Comparison of elasticities of Cu– C_{60} and C_{60} – C_{60} contacts

The forces at the junction cause atomic relaxations which affect the conductance. Below, a simple model is used to estimate the deformation of the junction from the measured conductance and force data. First, the conductance of a rigid junction is calculated as a function of the piezo displacement, $G_{\text{rigid}}^{\text{theo}}(\Delta z)$ [14] (for details see supplementary data, available from stacks.iop.org/NJP/14/073032/mmedia), which is shown in figure B.1. The junction deformation d is approximated by a linear relation $d = F(\Delta z)/k$, using the experimentally determined force $F(\Delta z)$. We then obtain the theoretical conductance of the deformed junction, $G_{\text{deform}}^{\text{theo}}(\Delta z)$, which depends on the stiffness of the junction k :

$$G_{\text{deform}}^{\text{theo}}(\Delta z) = G_{\text{rigid}}^{\text{theo}}\left(\Delta z - \frac{F(\Delta z)}{k}\right). \quad (1)$$

From a fit of $G_{\text{deform}}^{\text{theo}}(\Delta z)$ to the measured $G(\Delta z)$ data (figures 1(c) and 2(h)) the stiffness k is obtained. Figure 3(a) shows fits (solid lines) for Cu–h- C_{60} (crosses) and h- C_{60} –h- C_{60} (dots) contacts. Cu–p- C_{60} data (not shown) yield similar results. From measurements with different tips we determined elasticities $k \approx (16\text{--}37) \text{ N m}^{-1}$ for Cu– C_{60} and $k \approx (13\text{--}24) \text{ N m}^{-1}$ for C_{60} – C_{60} . The extracted deformation d shown in figure 3(b) corresponds to a reduction in the tip–molecule distance of $\approx 0.9 \text{ \AA}$ for the Cu– C_{60} contact (solid line). For the C_{60} – C_{60} contact (dashed line), d is smaller ($\approx 0.3 \text{ \AA}$) and the transition from tensile to compressive deformation occurs within the Δz range that was accessible in our experiment. While the deformations are smaller than the values reported for metal contacts [9, 32, 36], still they strongly affect the conductance.

The values for k may be interpreted in terms of the elasticities of the components of the junctions. DFT calculations taking into consideration several atomic configurations were used to estimate the elasticities of the tip and the sample (see appendix A). As summarized in table A.1, we find that a metallic Cu tip can be characterized by a stiffness in the range $k_{\text{Cu}}^{\text{tip}} \approx 45\text{--}55 \text{ N m}^{-1}$ depending on its atomistic structure and on the details of the calculational scheme. For the sample we find that $k_{\text{C}_{60}}^{\text{sample}} \approx 112\text{--}129 \text{ N m}^{-1}$ for h- C_{60} or p- C_{60} on reconstructed Cu(111) [22]. Combining tip and sample elasticities in series, we thus estimate $k_{\text{eff}} \approx 32\text{--}39 \text{ N m}^{-1}$ for a Cu– C_{60} contact. Similarly, for a h- C_{60} tip we find that $k_{\text{C}_{60}}^{\text{tip}} \approx 43\text{--}81 \text{ N m}^{-1}$, which leads to $k_{\text{eff}} \approx 31\text{--}50 \text{ N m}^{-1}$ for an h- C_{60} –h- C_{60} contact. For both contacts, the experimentally determined elasticity is softer than the calculated one by a factor of 2. We attribute this difference to two main factors: firstly, the elasticity calculations can be considered as upper bounds as only a finite number of degrees of freedom is taken into account (see appendix A). Secondly, the elasticity estimates above do not take into account the softening of the springs close to the contact due to the formation of chemical bonds between the tip and the sample.

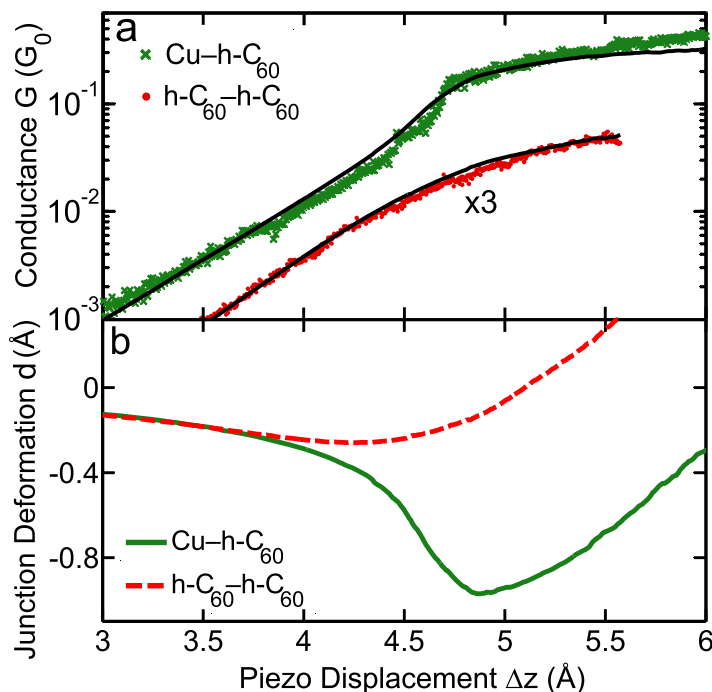


Figure 3. (a) Conductance G versus Δz during the formation of Cu-h-C₆₀ (crosses) and h-C₆₀-h-C₆₀ (dots) contacts. The solid lines are fits of $G_{\text{deform}}^{\text{theo}}$ to the measured conductance G using equation (1) with $k = 19.4 \text{ N m}^{-1}$ for Cu-h-C₆₀ and $k = 18.9 \text{ N m}^{-1}$ for h-C₆₀-h-C₆₀. Further details can be found in appendix B. (b) The junction deformation d extracted from the fits to $G(\Delta z)$ for Cu-h-C₆₀ (solid line) and h-C₆₀-h-C₆₀ (dashed line).

It is instructive to compare the obtained junction stiffness values with that of an isolated C₆₀ molecule. From our DFT calculations we find that squeezing a C₆₀ molecule between two opposite hexagons corresponds to a spring constant of 222 N m^{-1} (appendix A), i.e. the elasticity of a C₆₀ is significantly stiffer than the molecular junctions considered in this study. The junction deformation therefore mainly involves the metal-molecule bonds and the STM tip.

6. Conclusions

In summary, simultaneous force and conductance measurements for Cu-C₆₀ and C₆₀-C₆₀ contacts have been carried out. Angstrom-scale deformations of the contacts and effective stiffness extracted from the experimental data agree with elasticities determined with DFT calculations. We find that the maximal attractive force measured at a C₆₀-C₆₀ contact is four times smaller than in a Cu-C₆₀ junction. Moreover, the force data reveal that previously reported contact conductances correspond to geometries in which the junctions are under maximal tensile stress.

Acknowledgments

We thank C González and N L Schneider for discussions. Financial support from the Deutsche Forschungsgemeinschaft (SFB 677), the Innovationsfonds Schleswig-Holstein and the EU projects HERODOT and ARTIST is acknowledged.

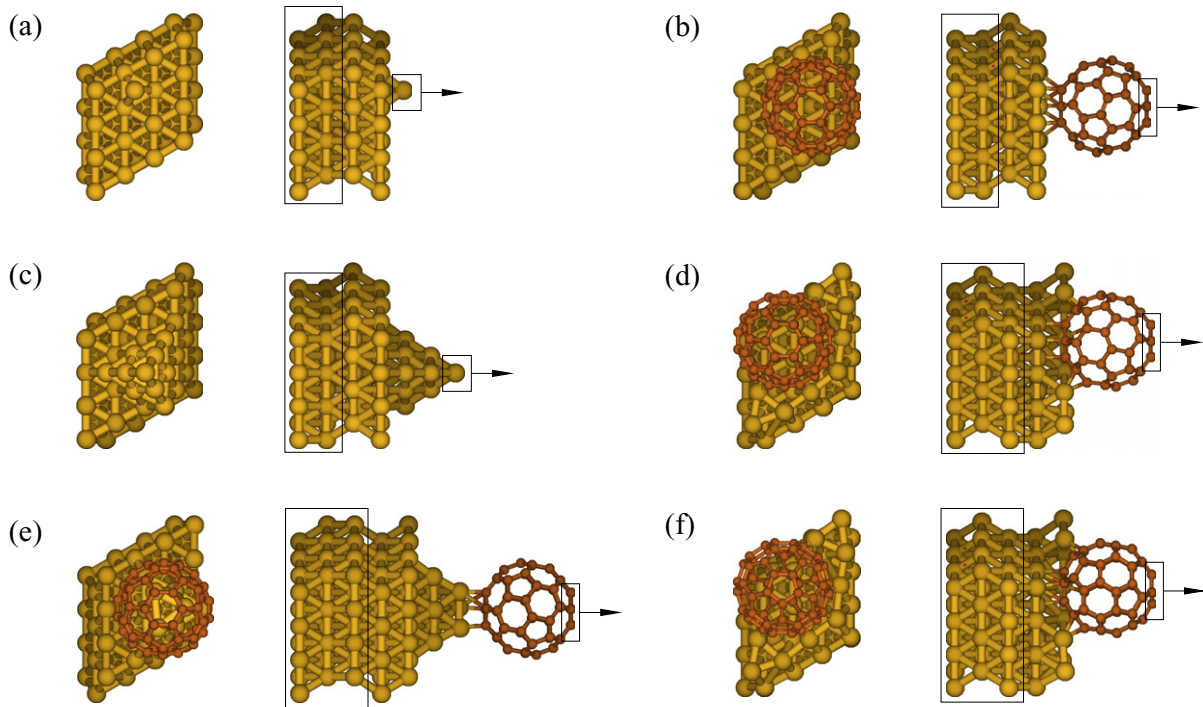


Figure A.1. Structures considered in the DFT calculations (top and side views): (a) Cu adatom on flat Cu(111), (b) h-C₆₀ on flat Cu(111), (c) pyramidal Cu tip, (d) h-C₆₀ on reconstructed Cu(111), (e) h-C₆₀ tip on Cu pyramid and (f) p-C₆₀ on reconstructed Cu(111). The boxed atoms in the (4 × 4)-Cu(111) slab are fixed at bulk coordinates, while the other degrees of freedom are relaxed. The elasticities are estimated from the energy increase associated with displacing the topmost atoms (box with an arrow) perpendicular to the surface film while allowing the remaining degrees of freedom to relax.

Appendix A. Density functional theory calculations

In order to estimate the elasticities related to the experimental sample and tip sides we considered the generic structures shown in figure A.1. Calculations were performed using the SIESTA [37] pseudopotential DFT method with the Perdew–Burke–Ernzerhof (PBE) functional [38] for the exchange–correlation energy within the generalized gradient approximation (GGA), a 400 Ry mesh cutoff and a 2 × 2 Monkhorst–Pack [39] k -mesh. The Fermi surface was treated by a second-order Methfessel–Paxton scheme [40] with an electronic temperature of 300 K. The basis set consisted of default double-zeta plus polarization (DZP) orbitals for C and Cu atoms generated with an energy shift of 0.01 Ry. The force tolerance for the structural optimizations was 0.02 eV Å^{−1}. The total energies from SIESTA were not corrected for basis set superposition errors. Two different lattice constants for the Cu crystal ($a = 3.62$ Å and $a = 3.70$ Å) were considered in order to confirm that the results do not depend sensitively on this parameter.

The computation procedure consisted of the following steps: (1) relaxation of the initial geometry with the boxed atoms in the Cu slab (figure A.1) fixed at bulk coordinates while the

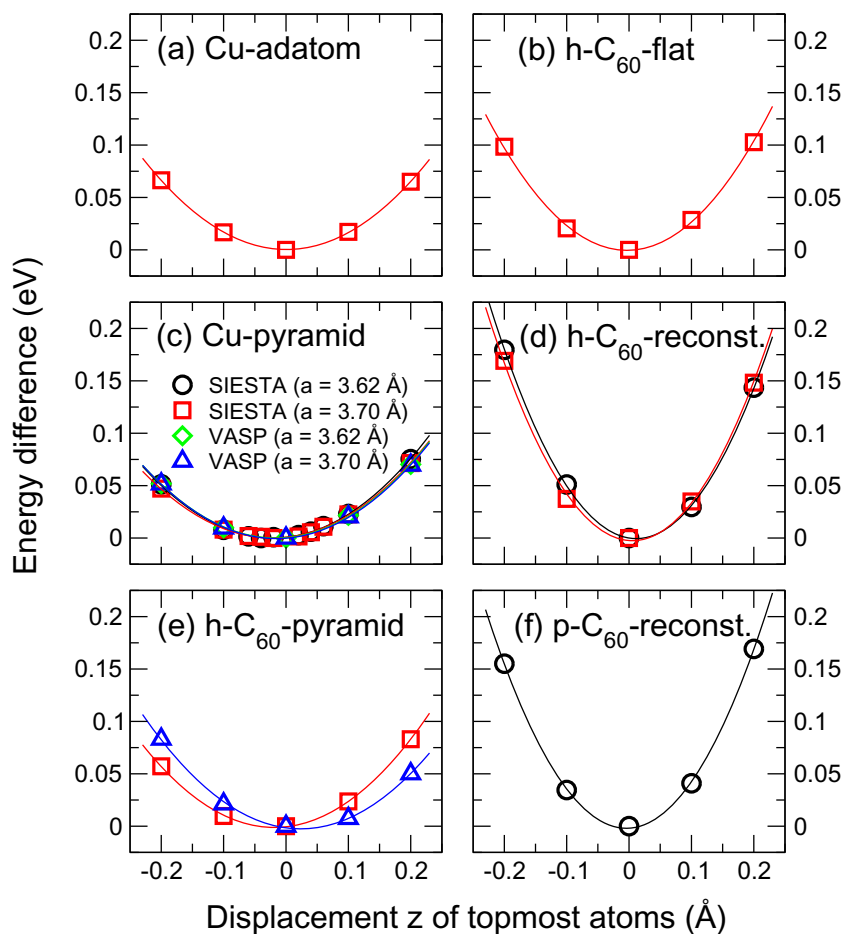


Figure A.2. Energy differences versus displacement z of the topmost atoms for the systems shown in figure A.1. The relaxed geometry corresponds to $z = 0$ Å, whereas the tensile strain is exerted on the system for $z > 0$ Å. The solid lines are quadratic fits to the calculated data points. The corresponding fitted spring constants are reported in table A.1.

other degrees of freedom are fully relaxed. (2) Displacement of the topmost atoms (box with an arrow in figure A.1) perpendicular to the surface film while relaxing all the remaining degrees of freedom.

The energy costs associated with deformations with respect to the displacement z of the topmost atoms are shown in figure A.2, with $z = 0$ Å being the relaxed junction. For $z > 0$ Å, tensile strain is exerted on the system. Quadratic (as well as fifth order) fits to these energy differences yield the effective spring constants in table A.1. It should be noted that the elasticities in table A.1 represent, in fact, upper bounds because of the limited size of the unit cell. In the real system, more atoms respond to the pull on the topmost atoms, which leads to a smaller effective spring constant.

To test the accuracy of the SIESTA calculations, selected checks with the VASP code based on a plane-wave basis and the projector-augmented wave method [41–43] were also performed. We used PBE-GGA [38], at least 400 eV energy cutoff, a 2×2 (or 3×3) Monkhorst–Pack [39] k -mesh, the first-order Methfessel–Paxton scheme [40] with 0.05 eV smearing width, and

Table A.1. Calculated spring constants k_{SIESTA} and k_{VASP} for the systems shown in figure A.1 using the SIESTA and VASP codes, respectively. The values in parentheses are derived from the second derivative of the fifth-order polynomial fits evaluated at the energy minimum. Two different lattice constants ($a = 3.62 \text{ \AA}$ and $a = 3.70 \text{ \AA}$) were considered for the Cu crystal. For comparison, the stiffness of an isolated C_{60} from figure A.3 is included.

Figure	System	a (\AA)	k_{SIESTA} (N m^{-1})	k_{VASP} (N m^{-1})
A.2(a)	Cu adatom	3.70	52 (55)	
A.2(b)	h- C_{60} flat	3.70	81 (78)	
A.2(c)	Cu pyramid	3.62	50 (44)	49 (51)
		3.70	47 (45)	49 (47)
A.2(d)	h- C_{60} reconst.	3.62	129 (129)	
		3.70	129 (112)	
A.2(e)	h- C_{60} tip	3.70	57 (53)	54 (43)
A.2(f)	p- C_{60} reconst.	3.62	131 (118)	
A.3	Isolated C_{60}		222 (240)	

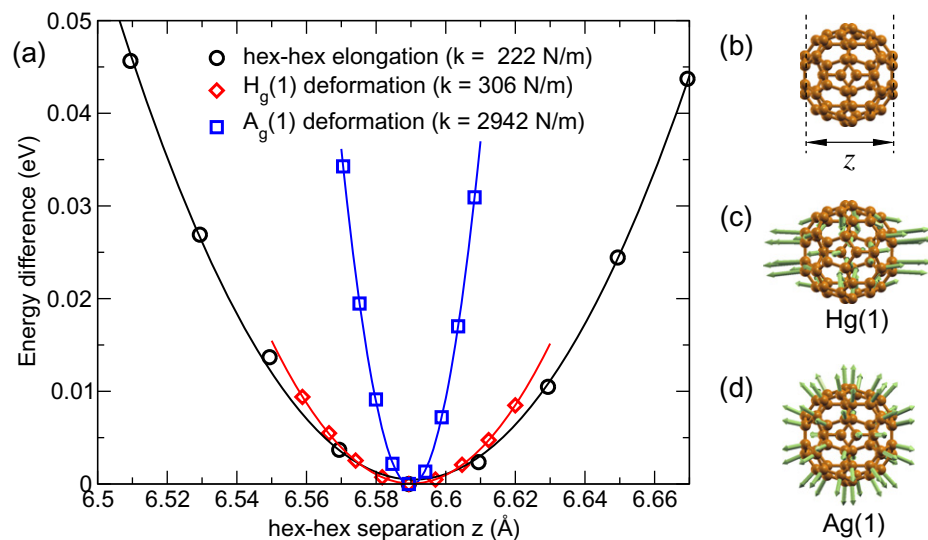


Figure A.3. (a) Energy differences versus hexagon–hexagon distance z for different deformations of an isolated C_{60} molecule. The solid lines are quadratic fits to the calculated data points. (b) Fixing the distance z between opposite hexagons while relaxing all other degrees of freedom (black circles). (c) $H_g(1)$ vibrational mode of C_{60} (compression/expansion, $\hbar\omega = 31 \text{ meV}$, red diamonds). (d) $A_g(1)$ vibrational mode of C_{60} (isotropic deformation, $\hbar\omega = 60 \text{ meV}$, blue squares).

0.02 eV \AA^{-1} force tolerance. As seen in figure A.2 and table A.1, the two codes yield similar estimates of the elasticities.

To determine effective elasticities for the combined elasticity of the tip and the sample the springs from table A.1 are added in series. In this way, for a Cu adatom (figure A.1(a)) or

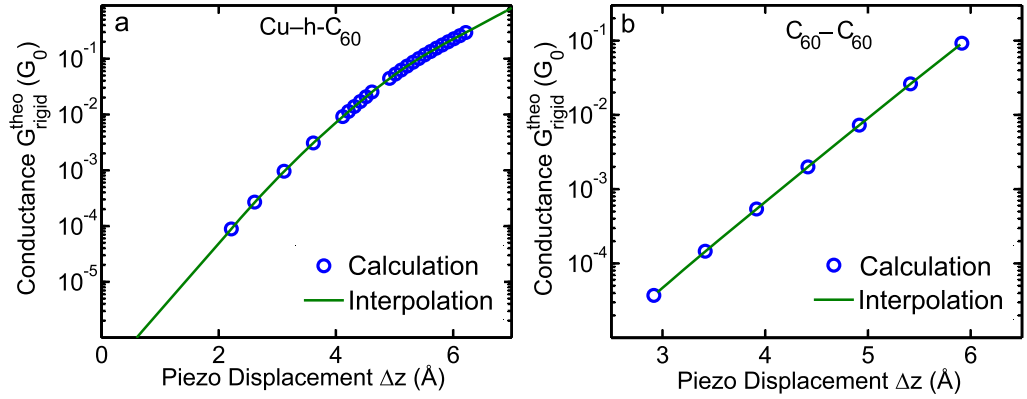


Figure B.1. Interpolated calculated conductance $G_{\text{rigid}}^{\text{theo}}$ as a function of the piezo displacement Δz for (a) Cu-h-C₆₀ and (b) C₆₀-C₆₀ contact. For the Cu-h-C₆₀ contact, $\Delta z = 0 \text{ \AA}$ corresponds to the distance between the topmost tip atom and the topmost C₆₀ hexagon of 8 \AA . For the C₆₀-C₆₀ contact, $\Delta z = 0 \text{ \AA}$ corresponds to a C₆₀-C₆₀ center distance of 14.9 \AA .

for a sharp pyramidal Cu tip (figure A.1(c)) in contact with an h-C₆₀ on reconstructed Cu(111) (figure A.1(d)), we obtain $k_{\text{eff}} = (1/k_{\text{tip}} + 1/k_{\text{surf}})^{-1} \approx 32\text{--}39 \text{ N m}^{-1}$. In the case of the contact between a Cu tip (figure A.1(a) or (c)) and an h-C₆₀ on the flat Cu(111) (figure A.1(b)), an effective elasticity of $k_{\text{eff}} \approx 29\text{--}33 \text{ N m}^{-1}$ is obtained. Due to the reduced number of bonds of h-C₆₀ on flat Cu(111) in comparison with h-C₆₀ on reconstructed Cu(111), k_{eff} is smaller. Similarly, for the C₆₀ tip (figure A.1(b) or (e)) in contact with an h-C₆₀ on reconstructed Cu(111), we estimate $k_{\text{eff}} \approx 31\text{--}50 \text{ N m}^{-1}$.

We also analyzed the stiffness of an isolated C₆₀ molecule with SIESTA, see figure A.3. By controlling the distance between two opposing hexagons while relaxing all other degrees of freedom, we obtain an effective stiffness of the molecule of $k_{\text{eff}} = 222 \text{ N m}^{-1}$. A comparable (but slightly larger) stiffness of $k_{H_{g1}} = 306 \text{ N m}^{-1}$ is obtained when considering only a deformation along the characteristic elongation/compression $H_g(1)$ vibrational mode (figure A.3(c)). Deforming along the isotropic $A_g(1)$ vibrational mode (figure A.3(d)) yields a much larger stiffness ($k_{A_{g1}} = 2942 \text{ N m}^{-1}$).

Appendix B. Elasticity model

The influence of the junction deformation on the conductance is described as follows. First, the conductance of a rigid system as a function of the piezo displacement, $G_{\text{rigid}}^{\text{theo}}(\Delta z)$, is calculated for Cu-h-C₆₀ and C₆₀-C₆₀ contacts (figures B.1(a) and (b)). $\Delta z = 0$ corresponds to a distance between the topmost tip atom and the topmost C₆₀ hexagon of 8 \AA in the Cu-h-C₆₀ contact and to a C₆₀-C₆₀ center distance of 14.9 \AA in the C₆₀-C₆₀ contact. Further calculation details can be found in [14].

Next, we assume that the deformation d depends linearly on the experimentally determined force, i.e. $d = F(\Delta z)/k$ with k describing the effective stiffness of the junction. The theoretical conductance of the deformed junction, $G_{\text{deform}}^{\text{theo}}(\Delta z)$, depending on k is given by

$$G_{\text{deform}}^{\text{theo}}(\Delta z) = G_{\text{rigid}}^{\text{theo}}\left(\Delta z - \frac{F(\Delta z)}{k}\right). \quad (\text{B.1})$$

The interpolated calculated conductance $G_{\text{deform}}^{\text{theo}}$ is then fitted to the experimental conductances $G(\Delta z)$. As the absolute tip–sample distance was unknown in the experiments, an arbitrary shift on the abscissa for $G_{\text{rigid}}^{\text{theo}}(\Delta z)$ is allowed. This shift is already included in figure B.1, so that the Δz axes in figures B.1(a) and (b) correspond to the axis in figure 3.

Fits for the Cu–h-C₆₀ and C₆₀–C₆₀ contacts shown in figure 3(a) and to similar data calculated for different microscopic tips yield $k \approx 16\text{--}37 \text{ N m}^{-1}$ and $k \approx 13\text{--}24 \text{ N m}^{-1}$, respectively. Compared to the values from the DFT calculations in appendix A, the effective spring constants qualitatively agree, but are smaller by a factor of 2. This deviation is not unexpected since the calculated elasticities are upper bounds. Furthermore, the model neglects the formation of chemical bonds between the tip and the sample, which are expected to weaken the effective spring constant.

References

- [1] Cross G, Schirmeisen A, Stalder A, Grütter P, Tschudy M and Dürig U 1998 *Phys. Rev. Lett.* **80** 4685
- [2] Rubio-Bollinger G, Joyez P and Agraït N 2004 *Phys. Rev. Lett.* **93** 116803
- [3] Limot L, Kröger J, Berndt R, Garcia-Lekue A and Hofer W A 2005 *Phys. Rev. Lett.* **94** 126102
- [4] Chen F, Hihath J, Huang Z, Li X and Tao N 2007 *Annu. Rev. Phys. Chem.* **58** 535–64
- [5] Néel N, Kröger J, Limot L, Frederiksen T, Brandbyge M and Berndt R 2007 *Phys. Rev. Lett.* **98** 065502
- [6] Schirmeisen A, Cross G, Stalder A, Grütter P and Dürig U 2000 *New J. Phys.* **2** 29
- [7] Sun Y, Mortensen H, Schär S, Lucier A S, Miyahara Y and Grütter P 2005 *Phys. Rev. B* **71** 193407
- [8] Sawada D, Sugimoto Y, Morita K, Abe M and Morita S 2009 *Appl. Phys. Lett.* **94** 173117
- [9] Ternes M, González C, Lutz C P, Hapala P, Giessibl F J, Jelínek P and Heinrich A J 2011 *Phys. Rev. Lett.* **106** 016802
- [10] Xu B, Xiao X and Tao N J 2003 *J. Am. Chem. Soc.* **125** 16164–5
- [11] Ebeling D, Oesterhelt F and Hölscher H 2009 *Appl. Phys. Lett.* **95** 013701
- [12] Lantz M A, O’Shea S J and Welland M E 1999 *Surf. Sci.* **437** 99–106
- [13] Fournier N, Wagner C, Weiss C, Temirov R and Tautz F S 2011 *Phys. Rev. B* **84** 035435
- [14] Schull G, Frederiksen T, Brandbyge M and Berndt R 2009 *Phys. Rev. Lett.* **103** 206803
- [15] Schull G, Frederiksen T, Arnau A, Sánchez-Portal D and Berndt R 2011 *Nature Nano* **7** 23–7
- [16] Pawlak R, Kawai S, Fremy S, Glatzel T and Meyer E 2011 *ACS Nano* **5** 6349–54
- [17] Pawlak R, Kawai S, Fremy S, Glatzel T and Meyer E 2012 *J. Phys.: Condens. Matter* **24** 084005
- [18] Schull G, Dappe Y J, González C, Bulou H and Berndt R 2011 *Nano Lett.* **11** 3142–6
- [19] Hashizume T *et al* 1993 *Phys. Rev. Lett.* **71** 2959
- [20] Pai W W, Hsu C, Lin M C, Lin K C and Tang T B 2004 *Phys. Rev. B* **69** 125405
- [21] Wang L and Cheng H 2004 *Phys. Rev. B* **69** 045404
- [22] Pai W W *et al* 2010 *Phys. Rev. Lett.* **104** 036103
- [23] Larsson J A, Elliott S D, Greer J C, Repp J, Meyer G and Allenspach R 2008 *Phys. Rev. B* **77** 115434
- [24] Sader J E and Jarvis S P 2004 *Appl. Phys. Lett.* **84** 1801–3
- [25] Sader J E and Sugimoto Y 2010 *Appl. Phys. Lett.* **97** 043502
- [26] Silien C, Pradhan N A, Ho W and Thiry P A 2004 *Phys. Rev. B* **69** 115434
- [27] Nonnenmacher M, O’Boyle M P and Wickramasinghe H K 1991 *Appl. Phys. Lett.* **58** 2921
- [28] Kitamura S, Suzuki K and Iwatsuki M 1999 *Appl. Surf. Sci.* **140** 265–70
- [29] Okamoto K, Sugawara Y and Morita S 2002 *Appl. Surf. Sci.* **188** 381–5
- [30] Israelachvili J N 1991 *Intermolecular and Surface Forces* 2nd edn (London: Academic)
- [31] Hobbs C and Kantorovich L 2006 *Surf. Sci.* **600** 551–8
- [32] Olesen L, Brandbyge M, Sørensen M R, Jacobsen K W, Lægsgaard E, Stensgaard I and Besenbacher F 1996 *Phys. Rev. Lett.* **76** 1485–8

- [33] Trouwborst M L, Huisman E H, Bakker F L, van der Molen S J and van Wees B J 2008 *Phys. Rev. Lett.* **100** 175502
- [34] Néel N, Kröger J and Berndt R 2011 *Nano Lett.* **11** 3593–6
- [35] Schneider N L 2012 private communication
- [36] Hofer W A, Fisher A J, Wolkow R A and Grütter P 2001 *Phys. Rev. Lett.* **87** 236104
- [37] Soler J, Artacho E, Gale J D, Garcia A, Junquera J, Ordejon P and Sanchez-Portal D 2002 *J. Phys.: Condens. Matter* **14** 2745–79
- [38] Perdew J P, Burke K and Ernzerhof M 1996 *Phys. Rev. Lett.* **77** 3865
- [39] Monkhorst H J and Pack J D 1976 *Phys. Rev. B* **13** 5188
- [40] Methfessel A and Paxton A T 1989 *Phys. Rev. B* **40** 3616
- [41] Kresse G and Hafner J 1993 *Phys. Rev. B* **47** 558
- [42] Kresse G and Furthmüller J 1996 *Phys. Rev. B* **54** 11169
- [43] Kresse G and Joubert D 1999 *Phys. Rev. B* **59** 1758